Chapter 4

Molecular Salts of Drug Famotidine with Isomeric Dihydroxybenzoic Acids

4.1 Abstract

This chapter demonstrates the stable solid-state formulations with desired properties for the labile drug famotidine (FAM) driven by conformational flexibility and ionizable nature. This drug is known for its bioavailability and stability issues. Six molecular salts with isomeric dihydroxybenzoic acids (DHBA) were synthesized through mechanochemical grinding followed by slow evaporation of solvents and characterized. These molecular salts exhibit improved stability under aqueous and various physiological pH conditions, which is attributed to the drug conformation change in the solid state. Such conformation modification eventually leads to strong hydrogen bond synthons with the conformers. Except for the anhydrous molecular salt with 26-DHBA, all others exhibit improved physicochemical properties viz. solubility, membrane permeation, and drug flux. The improvement of drug properties is endorsed by the formation of strong ionic guanidinium···carboxylate interactions between the API and coformers and the solute···solvent interactions. The difference in the isomeric position of OH groups, and the water molecule(s) of crystallization guided the formation of different auxiliary hydrogen bonds resulting in unique molecular packing with properties emphasized.

4.2 Introduction

Famotidine is an H_2-blocker class of medicine, commercially available under the brand name Pepcid [1]. It is a BCS class IV drug with very low oral bioavailability and stability issues. The formulation of multicomponent solids such as salts and cocrystals through crystal engineering techniques to improve the physicochemical and pharmacokinetic properties of the active pharmaceutical ingredient (API) has been an active research area for the last two decades [2–11]. Nangia et al. published recently an extensive review of the development of pharmaceutical cocrystals and their applications in the modulation of the different properties of drugs within the last two decades [12]. These methods improve the properties of the drug without altering its structural integrity. Apart from that cocrystallization techniques have gained wide interest because of their application in

the formulation of novel multidrug systems that exhibit a significant synergistic effect [13–15]. Reported studies also demonstrated the improvement of various stability issues of pharmaceutical compounds through the crystal engineering approach [16–21]. Cocrystals of vitamin K_3 with naphthoic acids and sulfamerazine have demonstrated superior photostability as compared to that of the marketed form [20]. The instability of an isoquinoline alkaloid berberine in high humidity was controlled via cocrystallization with fumaric acid [21]. The CSD search shows that few salts and cocrystals of FAM with improved physicochemical properties were reported (see Table 3.1 in Chapter 3). An antiulcer drug FAM rapidly degrades in highly acidic pH conditions. Cocrystals of FAM with xanthine derivatives demonstrated superior stability in simulated gastric and intestinal fluid [22]. In Chapter 3, we have discussed molecular salts of FAM with isomeric monohydroxybenzoic acids and isomeric monoaminobenzoic acids that showed better phase stability in three different physiological pH conditions. They also display different but improved solubility and permeation behaviors. The rationale for such variation in the properties is the strength of the acid···guanidine heterosynthon in the salt structures and the difference in the isomeric position of functional groups in the coformers that guided drug conformation change [23]. This chapter highlights the synthesis of six molecular salts for improved properties of the FAM with GRAS isomeric dihydroxybenzoic acids (Scheme 4.1). The ^{3}N (pK_a = 6.8) of guanidine moiety of the FAM acts as a hydrogen bond acceptor, whereas its two NH_2 groups act as hydrogen bond donors. The COOH group of DHBA can be either a hydrogen bond donor or an acceptor. The guanidine group of the FAM can form strong hydrogen bonds with the COOH group of DHBA.

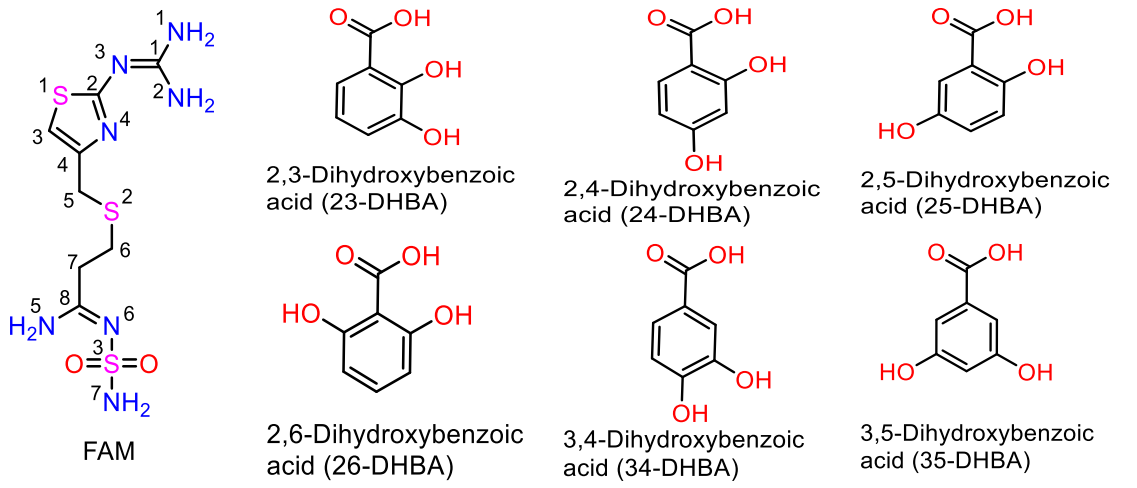

Scheme 4.1 Molecular structures of famotidine and isomeric dihydroxybenzoic acids.

The molecular salts are prepared to investigate how the isomeric positions of two phenolic OH groups in the coformers dictate the drug properties. This study focuses on how manipulating the noncovalent interactions that are responsible for the lipophilic nature and drug conformation adjustment can play a part in the modulation of the solubility and permeation behavior of the drug. The variation in the isomeric position of phenolic OH groups in the coformers together with the inclusion of water molecule(s) in the crystal lattice resulted in the formation of different hydrogen bonds and conformation change in the drug, which in turn led to a unique molecular packing of the salt with enhanced properties.

4.3 Results and Discussion

4.3.1 Synthesis of Molecular Salts

Isomeric dihydroxybenzoic acids that have antioxidant activity were selected to engineer multicomponent solids of the antiulcer drug famotidine (Scheme 4.1). Six molecular salts were prepared by mechanochemical grinding method and analyzed using spectroscopic, thermal, and X-ray diffraction techniques. As expected strong ionic hydrogen-bonded heterosynthon is formed between the guanidine moiety of the drug and the acid group of the coformers. Except for 26-DHBA, all the other coformers afforded solvated molecular salts with different solvent ratios (Table 4.1). All products were subjected to phase stability and physicochemical properties studies in three different pH conditions and compared with the parent API. The formation of different structure-forming hydrogen-bonded synthons and drug conformation change mediated the enhancement of the drug properties in these molecular salts.

Table 4.1 Crystallization of famotidine with isomeric dihydroxybenzoic acids leads to the formation of molecular salt hydrates and their respective stoichiometric ratio.

API	coformers	product	stoichiometric ratio	solvent
Famotidine (FAM)	2,3-Dihydroxybenzoic acid	F-23	1:1:2 [FAM:23-DHBA:H_2O]	MeOH & ACN
	2,4-Dihydroxybenzoic acid	F-24	1:1:1 [FAM:24-DHBA:H_2O]	MeOH
	2,5-Dihydroxybenzoic acid	F-25	1:1:1 [FAM:25-DHBA:MeOH]	MeOH
	2,6-Dihydroxybenzoic acid	F-26	1:1 [FAM:26-DHBA]	MeOH & ACN
	3,4-Dihydroxybenzoic acid	F-34	1:1:2 [FAM:34-DHBA:H_2O]	MeOH
	3,5-Dihydroxybenzoic acid	F-35	1:1:2.25 [FAM:35-DHBA:H_2O]	MeOH

4.3.2 Characterization of product phases

Vibrational Spectroscopy (FT-IR). The formation of pure bulk product materials was confirmed by FT-IR, DSC, TGA, and PXRD. The vibrational frequency for the N–H stretching of FAM appears at 3508 and 3237 cm^{-1}, whereas for all the product materials the N–H stretching peaks are observed in the lower range of 3425–3221 cm^{-1} (Figure 4.1). The lowering of N–H stretching peaks for all products suggests the formation of hydrogen bonding between the drug and coformers. The SO_2 absorption band of FAM which is observed at 1145 cm^{-1} displays a significant shifting of the peak for all the products (1118-1140 cm^{-1}), indicating its involvement in intermolecular interactions with coformers. The C=O vibration peaks for pure DHBA are observed near 1700 cm^{-1}. But, for all the product materials strong peaks appear in the carboxylate anion absorption regions (~1400 and ~1600 cm^{-1}), indicating the formation of salts due to the transfer of a proton from DHBA coformers to the drug.

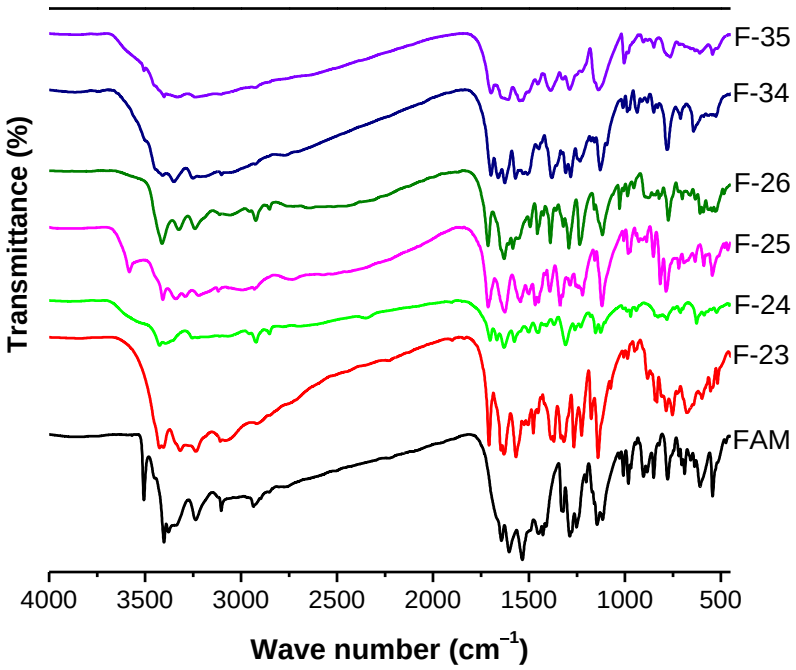

Figure 4.1 Vibrational spectroscopy of FAM and its molecular salts with isomeric DHBA.

Differential Scanning Calorimetry (DSC). The thermal property of the product materials is evaluated by DSC and TGA and are plotted in Figures 4.2 and 4.3 respectively. All the products display unique melting onsets which are different from the API and their respective coformers (Table 4.2). Among the products, F-26 displays a single endothermic transition in the range of 170–181 °C which suggests anhydrous product

formation. TG analysis also supports a non-solvated product formation for F-26 since the solvent loss peak is not observed. The DSC endotherms of the remaining products show a water loss peak before they melt which suggests the evaporation of the respective solvent molecules from their crystal lattice. All hydrated products display lower melting points than their respective starting materials. A close look at the single crystal structures of these hydrated products reveals that the solvent molecules in their crystal lattice serve as a linker between the drug–coformer heterodimers via weak hydrogen bonds. The solvent molecules are eliminated from the crystal lattice of salt hydrates due to evaporation at its boiling temperature and the systems undergo some rearrangement to form anhydrous solid forms [24].

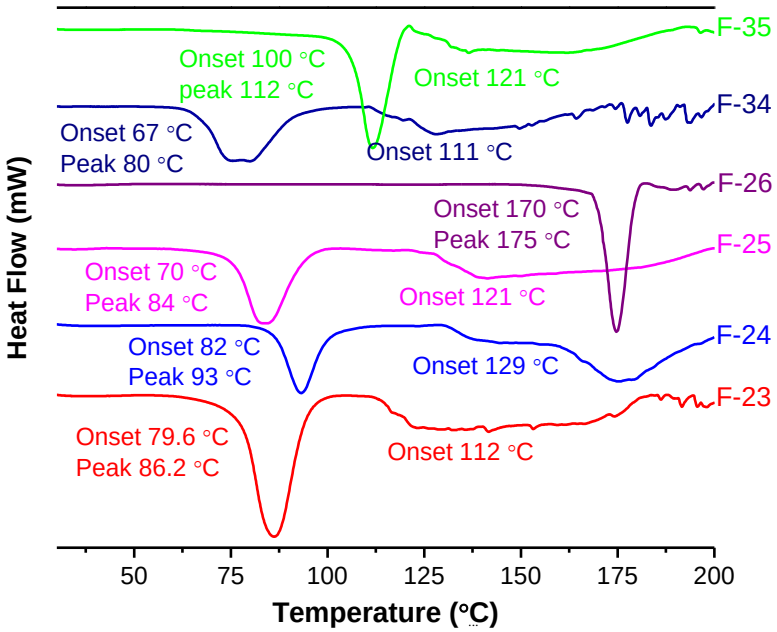

Figure 4.2 DSC thermograms of molecular salts of FAM with isomeric DHBAs.

Table 4.2 Comparison of DSC melting points of molecular salts with their respective starting materials.

API		coformers		solvent loss (°C)		salts Mt. Pt. (°C)	
Mt. Pt. (°C)	coformers	Mt. Pt. (°C)	Product	onset	peak	onset	peak
FAM (161-164 °C)	23-DHBA	204-206	F-23	79	86	112	130
	24-DHBA	208-211	F-24	82	93	129	decomposed
	25-DHBA	204–208	F-25	70	84	121	141
	26-DHBA	165-167	F-26	-	-	170	175
	34-DHBA	197-200	F-34	67	80	111	128
	35-DHBA	236–238	F-35	100	112	121	decomposed

Thermogravimetric Analysis (TGA). The number of solvent molecules present in these hydrated salts was predicted by the TGA and found to be consistent with the

stoichiometric ratio determined by X-ray crystal structure analysis (Figure 4.3). The percentage of weight loss which is observed in the TG endotherm of products between 65 and 125 °C indicates dihydrate structure for F-23 (obs. 6.78%, calc. 6.83%), F-25 (obs. 6.74%), and F-34 (obs. 6.75%, calc. 6.83%), and a monohydrate structure for F-24 (obs. 3.43%, calc. 3.52%). Similarly, the evaporation of 2.25 molecules of water from the crystal lattice of F-35 (obs. 7.42%, calc. 7.63%) is predicted by TG analysis. For most hydrated products, the release of water molecules stays up to 125 °C. The water molecules of crystallization in those salts are hydrogen bonded with the drug and/or coformer via the strong ionic N^{+}–H···O and O–H···O^{-} interactions.

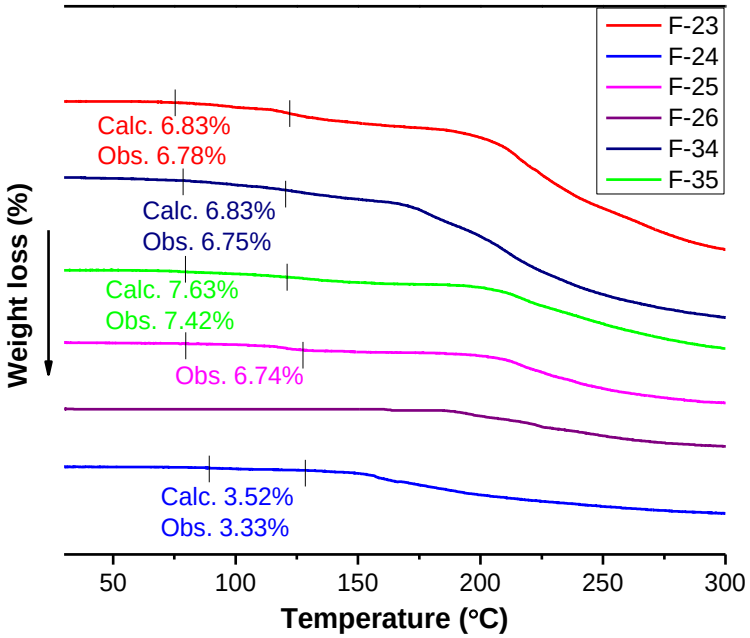

Figure 4.3 The observed weight loss measured by TGA is consistent with the 1:1:2 for dihydrates (F-23, F-25, and F-34), 1:1:2.25 for F-35, and 1:1:1 for monohydrate (F-24) ratios obtained from X-ray crystal structural analysis.

Powder X-ray Diffraction (PXRD). The PXRD patterns of the bulky powder samples of F-23 to F-35 are compared with their respective starting materials and found to be different from them (Figure 4.4). The phase purity and homogeneity of the product materials are analyzed by comparing the experimental and simulated PXRD patterns. Rietveld refinement was carried out for each product using Powder Cell 2.3 software to overlay the experimental PXRD pattern with its respective simulated pattern extracted from the single crystal structures. The bulky PXRD patterns and intensity for all six products match well with their respective simulated profile (Figure A5, Appendix). This

shows the formation of pure and homogenous multicomponent crystalline materials from the API and coformers by co-grinding.

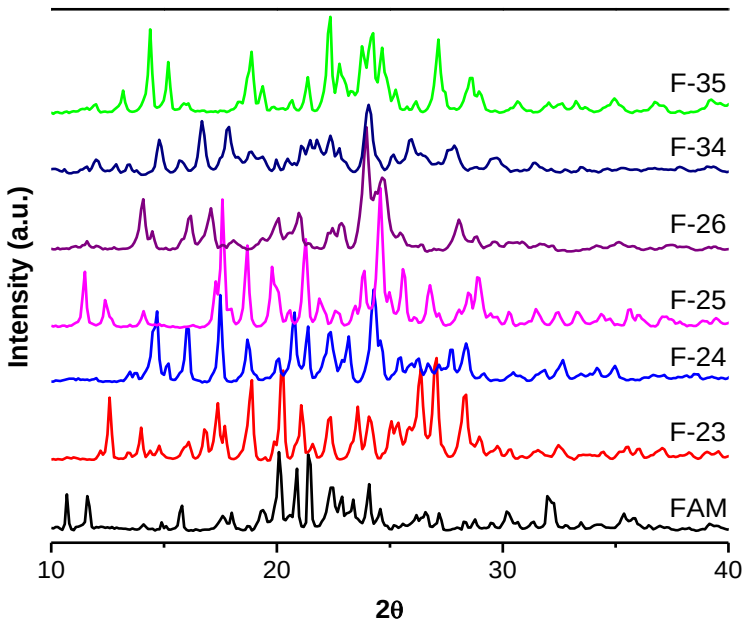

Figure 4.4 PXRD patterns of molecular salts F-23 to F-35 along with the parent API.

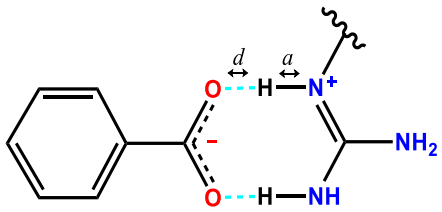

Figure 4.5 The prime guanidinium···carboxylate supramolecular heterosynthon in the molecular salts F-23 to F-34.

Table 4.3 The pK_a values of API and coformers. The observed acid hydrogen distance parameters from donor (*d*) and acceptor (*a*) atoms are calculated from the single crystal structure of the products (Figure 4.5).

pK_a value of API	coformers	pK_a value of coformers	acid-base ΔpK_a	product	distance (Å)		solid form
					d	*a*	
	23-DHBA	2.91	3.89	F-23	-	0.88	Salt
	24-DHBA	3.11	3.69	F-24	1.89	0.88	Salt
FAM	25-DHBA	2.97	3.83	F-25	1.80	0.88	Salt
(6.8)	26-DHBA	1.51	5.29	F-26	1.80	0.88	Salt
	34-DHBA	4.26	2.54	F-34	1.82	0.88	Salt
	35-DHBA	4.04	2.76	F-35	-	0.86	Salt

The ΔpK_a rule of three helps to forecast the formation of cocrystals or salts for the product materials. The ΔpK_a values are in the unpredictable region of cocrystal or salt formation, except for 26-DHBA which falls in the salt formation region (Table 4.5). Thus, either a complete proton transfer or formation of salt–cocrystal continuum was expected between FAM and coformers. The single crystal structural analysis discussed in the subsequent section confirms the exact position of the proton in these product materials. The crystal structures of F-23 and F-35 show that the acid proton is completely transferred to the basic N atom of the guanidine moiety of the FAM and forms a hydrogen bond with the water molecule in the crystal lattice, confirming the formation of salt hydrates. In the remaining products, the proton is located near the basic N atom of the guanidine moiety rather than the originally bound oxygen atom of COOH which is an indication of salt formation. But it remains hydrogen-bonded to the oxygen atom of the acid (Figure 4.5). Apart from that the increase in the bond length and bond angle of the imine group in the guanidine moiety of the drug (C1–N3 = 1.33 Å and C1–N3–C2 = 120.12° for unprotonated FAM-A to 1.35–1.37 Å and 125.08–126.63° for the product materials) indicates guanidine cation formation. Similarly, the bond length and angle parameters of the carboxylic acid group in DHBA are also as expected for the salts (Table A6, Appendix).

Single Crystal X-RD. Crystals suitable for the single crystal data collection are obtained from solution crystallization of ground materials in methanol (MeOH) or solvents mixture of MeOH and acetonitrile (ACN). The single crystal structure determination shows that all the products have solvent molecules in their crystal lattices except F-26. The single crystals for F-23 were obtained by slow evaporation from the mixture of MeOH and ACN. The crystal structure is solved and refined in triclinic space group $P\bar{1}$ with one FAM, one 23-DHBA, and two H_2O symmetry-independent molecules. A complete transfer of proton occurred from a carboxylic acid to the basic N atom on the imine moiety of the drug. The carboxylate anion of 23-DHBA and guanidine of FAM form a $R_2^2(8)$ heterodimer ring motif via N^+–H···O^- and N–H···O interactions (Figure 4.6a). Water molecules in the crystal lattice are linked by O–H···O hydrogen bonding to form a cyclic tetramer (Figure 4.6b). The heterodimers are arranged in parallel along the crystallographic *b*-axis by O–H···O hydrogen bonds from water molecules to COO^- a group of 23-DHBA with the support of N–H···O hydrogen bonding from protonated

imine group of guanidine moiety to the oxygen atom of water. The structure is extended in 2D by the formation of homodimer $R_2^2(12)$ ring motif through N–H···O hydrogen bonding along the *c*-axis.

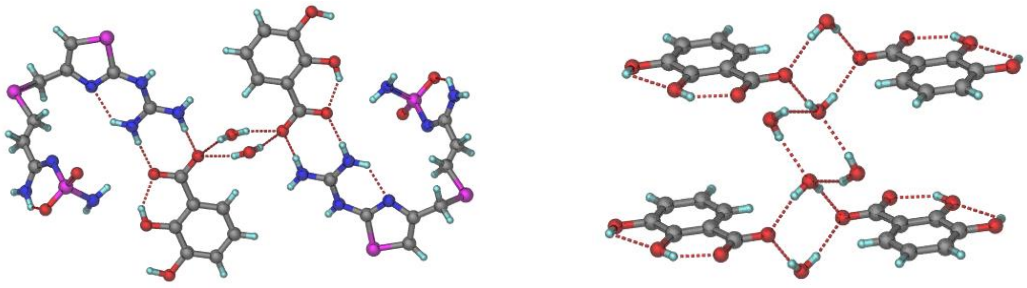

(a) (b)

Figure 4.6 (a) In F-23, symmetrical independent FAM molecules which are connected with 23-DHBA by N^+–H···O^- hydrogen bonds form guanidinium···COO^- supramolecular heterodimers. Such dimers are linked by water molecules via O–H···O interactions. (b) Water tetramer in the voids of F-23 interacts with 23-DHBA by O–H···O hydrogen bonds.

Single crystals of F-24 were obtained by dissolving ground powder material in MeOH and kept for crystallization for 3-4 days. It crystallizes in the monoclinic system of the *P*21/c space group with a ratio of 1:1:1 for each FAM, 24-DHBA, and water molecule. In the crystal structure of F-24, the two OH groups of symmetry-independent 24-DHBA molecules are joined in zigzag motion by the water molecule via O–H···O hydrogen bond to form a 1D molecular tape. Two inversion-related FAM molecules are linked by N–H···O interactions to form a dimer. These dimers are further connected by $N–H_{(sulfonamide\ NH2)}\cdots N_{(amidine\ C=N)}$ hydrogen bonds to form 1D molecular chains. The structure extends in a 2D via a $R_2^2(8)$ ring motif formation between FAM and 24-DHBA (Figure 4.7).

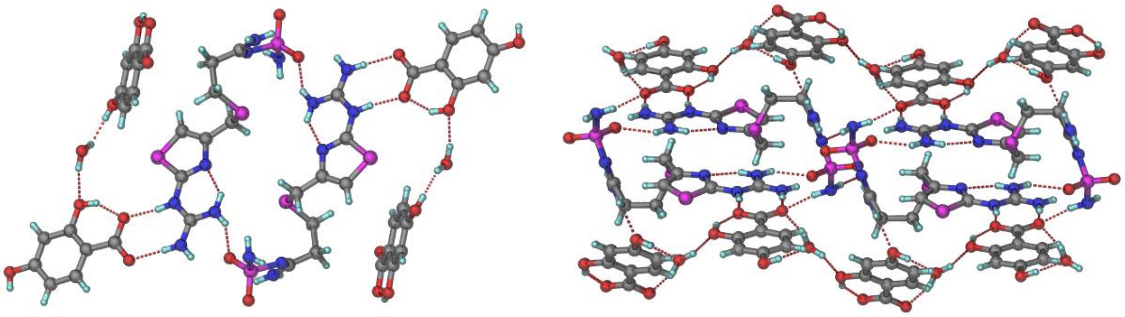

(a) (b)

Figure 4.7 (a) FAM homodimer is connected with 24-DHBA molecular tape via $R_2^2(8)$ ring motif to form (b) a 2D molecular packing in the crystal structure of F-24.

Similarly, single crystals of F-25 salt were harvested from the MeOH solvent. It crystallizes in a monoclinic space group *P*n with one molecule of FAM, 25-DHBA, and MeOH. In F-25, a $R_2^2(8)$ supramolecular heterodimers formed from FAM and 25-DHBA through N–H···O and N^+–H···O^- hydrogen bonds are connected by $N–H_{(amidine\ NH2)}\cdots O_{(meta\ OH)}$ and $N–H_{(sulfonamide\ NH2)}\cdots O_{(COO^-)}$ interactions to construct 1D molecular tape. The tapes are associated by MeOH molecules via O–H···O interactions and supported by $N–H_{(guanidine\ NH2)}\cdots O_{(ortho\ OH)}$ interactions to form a 2D sheetlike structure (Figure 4.8). The presence of MeOH solvent in the pharmaceutical solids formulation is not recommended by regulatory agencies. However, the single crystal structure determination of the MeOH-solvated salt product of F-25 was carried out to understand the intermolecular interactions. The drug property evaluation was performed directly using ground powder samples in which the formation of salt hydrates was confirmed by the PXRD, DSC, and TGA analysis. The attempt to obtain crystals suitable for the single crystal X-RD data collection was not successful for the hydrated form of F-25.

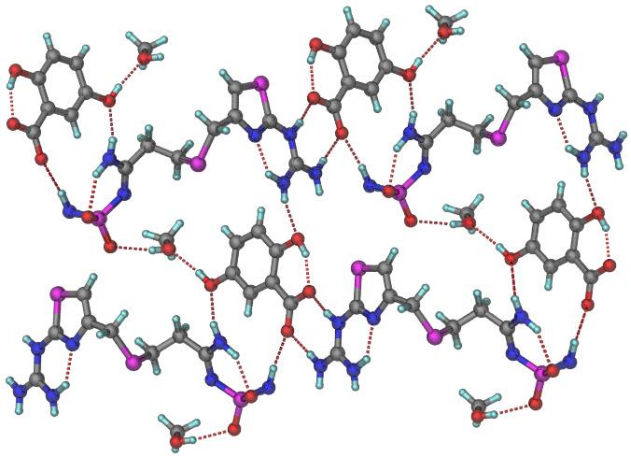

Figure 4.8 MeOH molecules serve as a linker between the drug–coformer dimers to form a 2D structure in the F-25.

Single crystals of F-26 with diffraction quality were produced by slow crystallization of ground powder sample in a solvent mixture of MeOH and ACN. In the crystal structure of F-26 (1:1, monoclinic, *C*c), drug–conformer dimers are associated through N–H···O hydrogen bonds from NH_2 group of guanidine to the oxygen atom of sulfonamide moiety and NH_2 group of amidine to OH of 26-DHBA to form a 2D sheetlike layers (Figure 4.9). These layers are interconnected via the N–H···O hydrogen bond which is formed between sulfonamide groups of two FAM molecules.

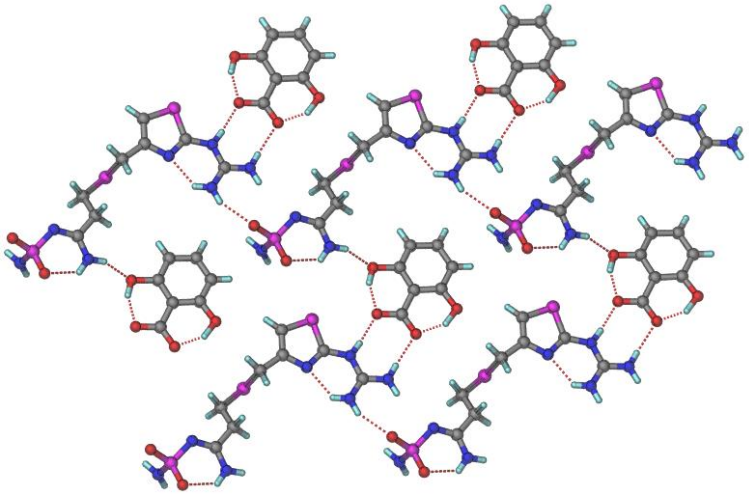

Figure 4.9 The 2D sheets in the F-26 are connected by N–H···O hydrogen bonds.

Good quality crystals of both F-34 and F-35 were obtained from crystallization in MeOH solvent. The crystal structure of F-34 (1:1:2, monoclinic, *C*2/c) reveals that the drug–coformer dimers are connected by water molecules via O–H···O interactions to form chains that extend further into 2D sheets (Figure 4.10a). Product F-35 crystallizes in the monoclinic space group of *P*21/c with the composition ratio of 1:1:2.25 of FAM, 35-DHBA, and water respectively. The crystal structure of F-35 displays analogous molecular packing in the crystal lattice as it is observed in the F-24 crystal structure. An inverted dimer of FAM molecules is formed in both crystal structures. The fundamental difference between the two crystal structures is that the functional groups of FAM that involve in hydrogen bonding with the carboxylate group of coformers. Unlike the others, the COO^- group of 35-DHBA is hydrogen bonded to NH_2 of the amidine moiety of FAM and the OH group of another neighboring 35-DHBA while one of its OH groups forms a hydrogen bond with the NH_2 group of the guanidine moiety (Figure 4.10c). Such drug-coformer interactions in F-35 lead to the formation of voids for more solvent molecules inclusion**.** Two water molecules form a dimer and serve as a linker for the drug dimers to form a 1D molecular chain. The remaining 0.25 water molecule connects the 35-DHBA molecules to form 1D molecular tape. The molecular tapes of drug and coformer are connected through N–H···O^- and N–H···O hydrogen bonds to form a 2D sheetlike structure of F-35 (Figure 4.10d).

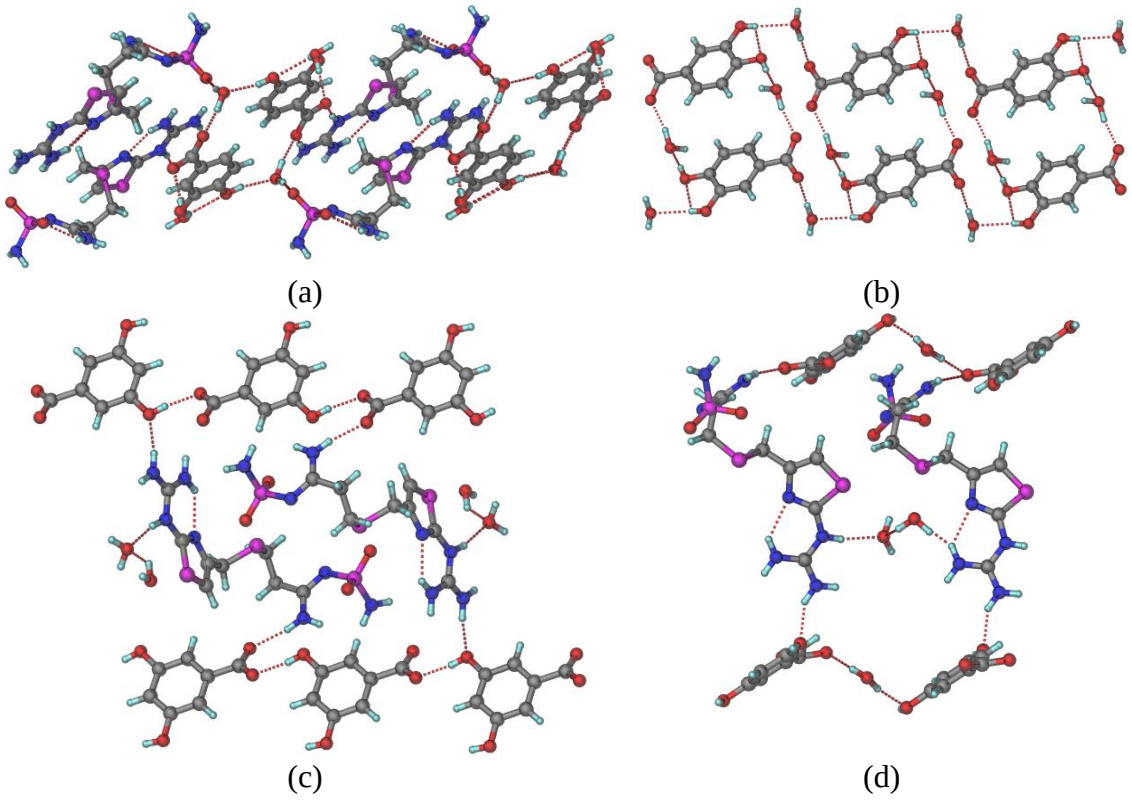

Figure 4.10 (a) Dimers in the crystal structure of F-34 are connected by water molecules. (b) 34-DHBA molecules are connected by water molecules to form a 1D molecular chain. (c) F-35 structure with N–H···O$^-$, N–H···O, and O–H···O$^-$ interactions. (d) Water dimers in the voids held by O–H···O hydrogen bonds connect the drug dimers via N–H···O$^-$ and N–H···O interactions. One of the FAM molecules that forms an inverted dimer is removed for clarity of the diagram.

Table 4.4 Important hydrogen bond parameters observed in the salts F-23 to F-35.

Salts	Interaction	H···A (Å)	D···A (Å)	∠D–H···A (°)	Symmetry Code
F-23	N1–H1A···O3	1.88	2.867(10)	157	-1+x, 1+y, z
	N2–H2A···O4	1.91	2.926(10)	167	-1+x, 1+y, z
	N3–H3···O7	1.84	2.823(10)	157	1-x, 1-y, 1-z
	N7–H7C···O4	2.20	3.231(11)	174	x, 1+y, z
	O7–H7E···O8	1.88	2.827(11)	162	1-x, 1-y, 1-z
	O8–H8B···O3	1.79	2.756(11)	167	-1+x, y, z
F-24	N1–H1B···O3	1.82	2.858(4)	175	-1+x, 1/2-y, -1/2+z
	N3–H5···O4	1.73	2.757(4)	169	-1+x, 1/2-y, -1/2+z
	N5–H8A···O6	2.05	3.082(4)	173	1+x, y, z
	N7–H9A···N6	1.99	3.009(4)	167	2-x, -y, 2-z
	N7–H9B···O3	1.88	2.895(5)	167	2-x, -1/2+y, 3/2-z
	O6–H12···O7	1.78	2.755(5)	173	x, 1/2-y, 1/2+z
F-25	N1–H1B···O3	1.78	2.811(6)	178	1+x, y, z
	N3–H3···O4	1.65	2.668(5)	168	1+x, y, z
	N7–H9A···O1	1.97	3.007(6)	175	1+x, y, z

	N7–H9B···O3	1.92	2.951(6)	171	x, -1+y, z
	O6–H12···O15	1.65	2.619(7)	167	1+x, 1+y, z
	O15–H16···O2	1.87	2.846(7)	173	-1/2+x, -y, 1/2+z
F-26	N1–H1A···O3	1.83	2.857(16)	169	x, 1+y, z
	N3–H3···O4	1.65	2.674(15)	169	x, 1+y, z
	N5–H8A···O6	1.86	2.815(17)	151	-1/2+x, 1/2+y, -1+z
	N7–H9A···O5	2.16	3.084(17)	147	-1/2+x, 1/2-y, -1/2+z
	N7–H9B···O1	1.98	3.000(15)	168	x, -y, 1/2+z
F-34	N1–H1B···O3	1.78	2.7989(19)	166	1-x, -y, 1-z
	N3–H3···O4	1.67	2.6877(18)	167	1-x, -y, 1-z
	O6–H6···O8	1.76	2.731(2)	169	
	O7–H15···O7	1.77	2.724(2)	164	1-x, y, 1/2-z
	O7–H16···O4	1.70	2.6851(17)	179	x, 1+y, z
F-35	N2–H2A···N6	2.31	3.167(6)	164	1-x, 1/2+y, 3/2-z
	N3–H3A···O7	2.00	2.862(8)	167	x, 1+y, z
	O5–H5E···O4	1.78(6)	2.561(5)	170	x, -1+y, z
	O6–H6C···O8	1.84(7)	2.618(5)	161	1+x, -1+y, z
	O8–H8C···O3	1.80(4)	2.685(5)	176	1-x, 1-y, 2-z
	O8–H8D···O6	1.91(5)	2.787(5)	168	1-x, 1/2+y, 3/2-z

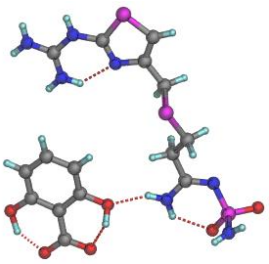

Synthon A (observed in F-26)

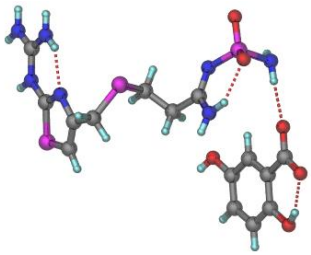

Synthon B (observed in F-25)

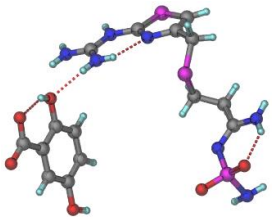

Synthon C (observed in F-25)

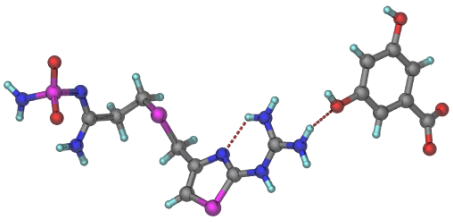

Synthon D (observed in F-35)

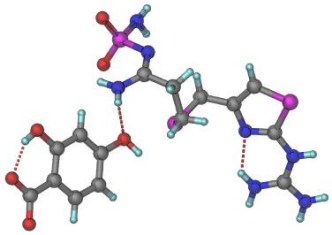

Synthon E (observed in F-24 and F-25)

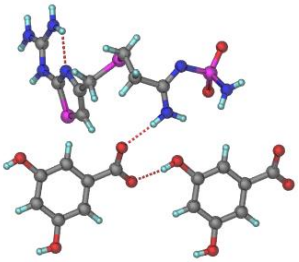

Synthon F (observed in F-35)

Figure 4.11 Various hydrogen bonding interactions observed in the crystal structures of F-23 to F-35.

The single crystal structural analysis discussed in the above section reveals that each product material has a unique molecular packing because of the differences in the hydrogen bonds formed between the drug and coformers (Figure 4.11) and drug conformation in the crystal lattices. An overlaid molecular conformers of FAM extracted from the single crystal structures of the molecular salts show a significant variation in the conformation of the drug molecule (Figure 12). Essentially, the isomeric positions of OH groups in the coformers play a key role in changing the drug conformation as they involve in the hydrogen bonding to support the molecular packing in the multicomponent solids. Because of the presence of flexible methylene and ethylene groups which connect –S2– with the thiazole and amidine moieties respectively, FAM molecule can easily adopt various molecular conformations by changing its torsion angles to interact well with different isomeric coformers of DHBA (Figure 13 and Table A7, Appendix). Such conformation change may render better stability and physicochemical properties for the drug in different physiological pH conditions which are discussed herein.

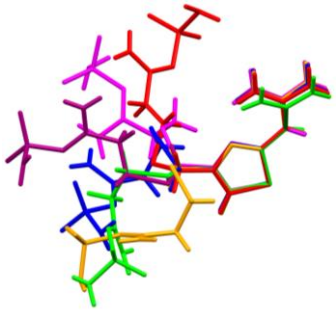

Figure 4.12 An overlay of molecular conformers of FAM extracted from the single crystal structures of products F-23 to F-35. [F-23 (red), F-24 (blue), F-25 (magenta), F-26 (purple), F-34 (orange), and F-35 (green)].

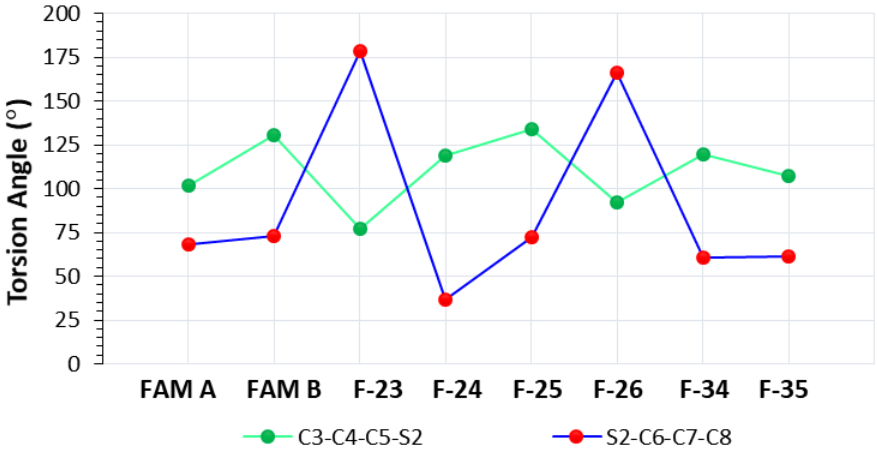

Figure 4.13 The observed conformational deviation in drug molecules in the crystal structures of F-23 to F-35 via two different torsion angles of the flexible moiety of the FAM structure referred to in Scheme 4.1.

4.3.3 Stability Study

The stability of each product in pure water and at pH 1.2 and 7.4 media was validated by PXRD analysis before doing a physicochemical properties study (Figure 4.14). The phase stability experiments were carried out according to the procedures reported in the literature [25]. In an aqueous medium, among the products only the sample of anhydrous salt F-26 retrieved after 24 h exhibited a minor change in the PXRD profile since few new peaks appeared. The appearance of new additional peaks shows the transformation of phase which is an indication of its unstability after 24h in the aqueous medium. Similarly, F-24 and F-26 are not stable at a pH 7.4 medium since their PXRD patterns show gradual change within a time frame of 24 h (Figure 4.14b, d). The stability of remaining salts was checked for up to 24 h and found to be stable in both media. The stability experiment for the products was also done at pH 1.2. Although FAM has a stability issue in acidic conditions, the PXRD profiles of all the six multicomponent solids were found to be consistent up to 24 h at pH 1.2 (Figure 4.14), confirming the enhancement of the drug stability via salt formation with coformers through strong hydrogen bonded supramolecular heterosynthons. The single crystal structure analysis of the products shows that the interaction of drug FAM with the isomeric DHBA coformers has changed the drug molecular conformation in different ranges of torsion angle (Table A7, Appendix). For instance, the torsion angle in the acid-sensitive amidine group of FAM ($^{8}C–^{6}N–^{3}S–^{7}N$) in the structure of FAM-A and FAM-B is 59.3 and 67.9° respectively. This angle increases to 163° in the F-24 and lies in the range of 80–87° for the remaining salts. Such change in the geometry of the amidine moiety of FAM molecule due to salt formation may avert the sensitive basic site, –C=N–, from acid hydrolysis, which might be one of the possible reasons for the observed better stability.

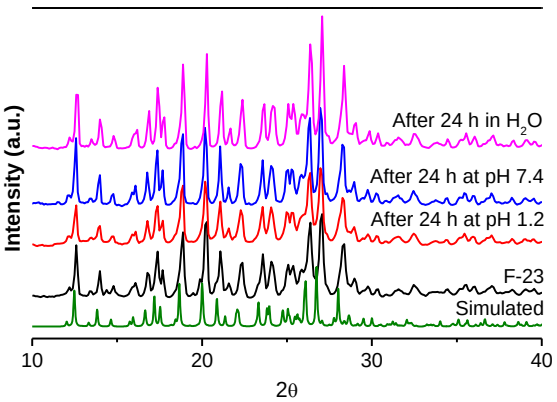

(a) F-23

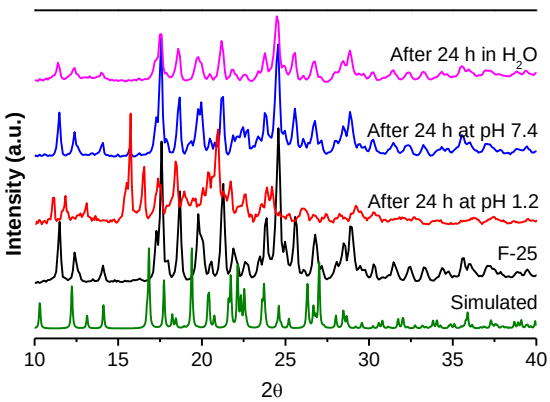

(c) F-25

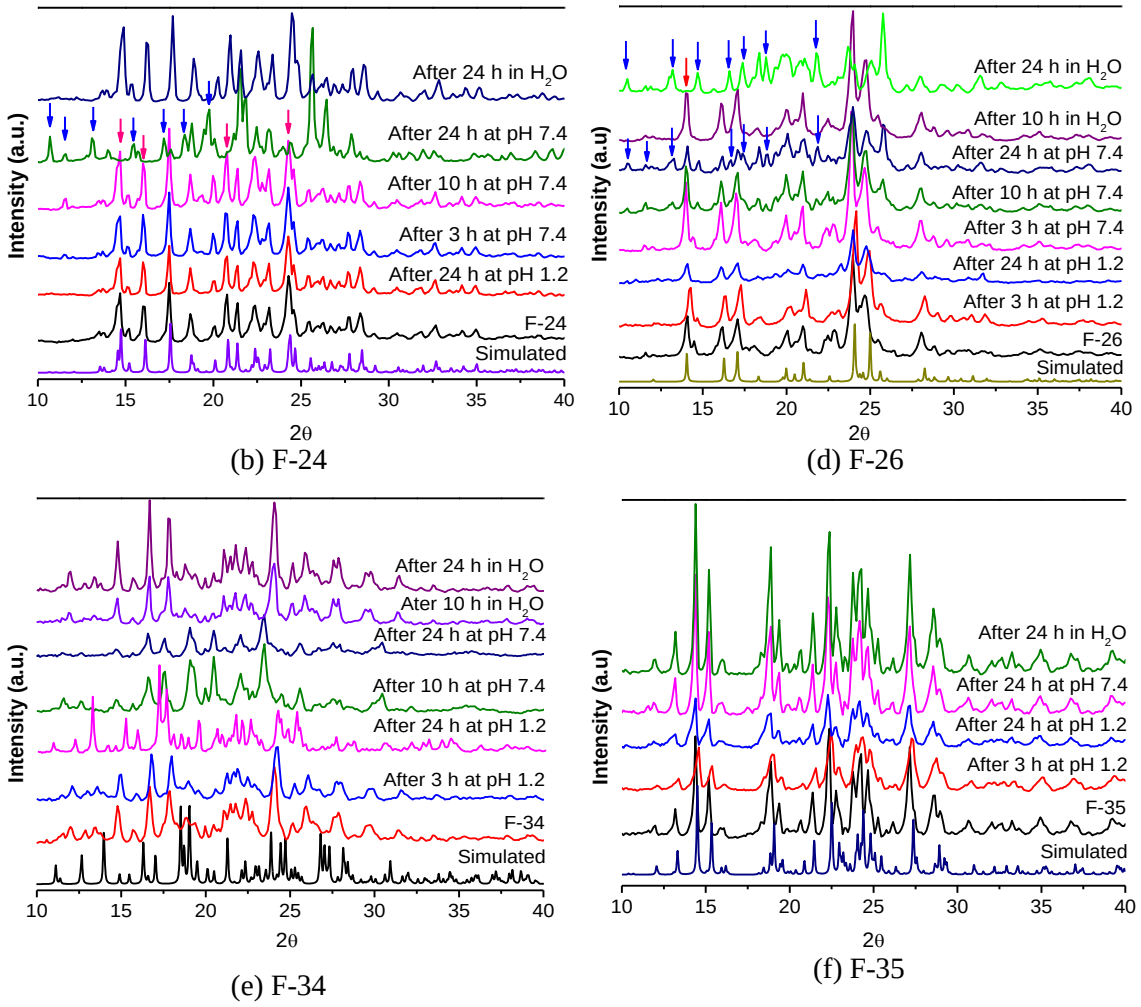

Figure 4.14 The phase stability test of molecular salts of FAM in pure water and at pH 1.2 and 7.4 conditions. Except for F-24 and F-26 at pH 7.4 and F-26 in aqueous media, the PXRD profiles of the samples of the remaining salts extracted from the slurry experiment of the three different media within 24 h match well with their respective simulated PXRD profile, suggesting the stability of these products.

Apart from the change in the overall conformation of the drug molecule, the inclusion of water molecules in the crystal lattice also improved the phase stability of the product materials by providing a stable molecular packing for the system. From the phase stability study via slurry experiment we observed that monohydrated F-24 salt at pH 7.4 and anhydrous F-26 salt in both aqueous and 7.4 pH media displayed slight phase change at 24 h, whereas the rest four dihydrated salts did not show phase change in all the three media. The calculated packing energy for the salt dihydrates (F-23, F-34, and F-35) is higher than that of the monohydrated F-24 and anhydrous F-26 salts which signifies the inclusion of a higher number of water molecules in the crystal lattice renders a better molecular packing for those salts.

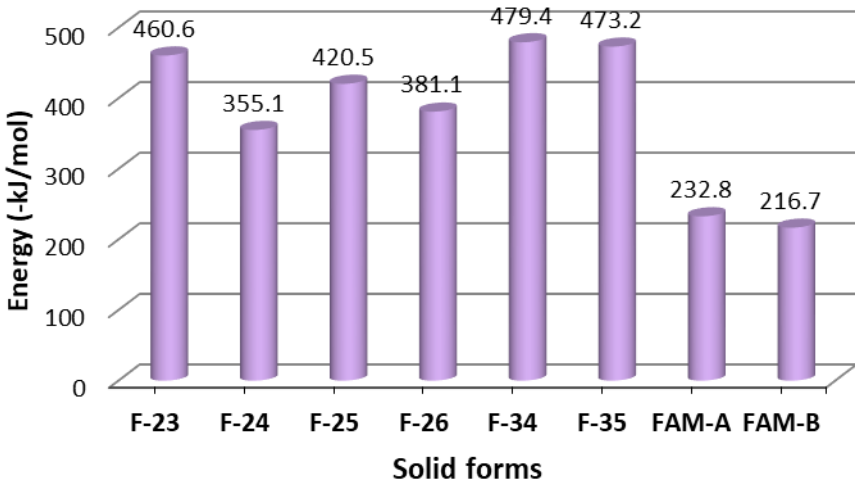

Figure 4.15 The crystal packing energy of the FAM and its salts, F-23 to F-35.

4.3.4 Solubility Determination in different pH media

Solubility is one of the essential parameters that determine the overall bioavailability of orally administered medicines. Among the various multicomponent solid formulation techniques which are used to overcome the solubility issue of drugs, salt formation is the most preferred method because of its high stability and solubility [26]. Here, it is important to mention that solid dosage forms of oral medicines can have different solubility in different physiological pH conditions. Hence, the solubility experiment of FAM and its molecular salts was done in pure water (pH ~7.0) and simulated stomach (pH ~1.2) and intestinal (pH ~7.4) fluids (Figure 4.16).

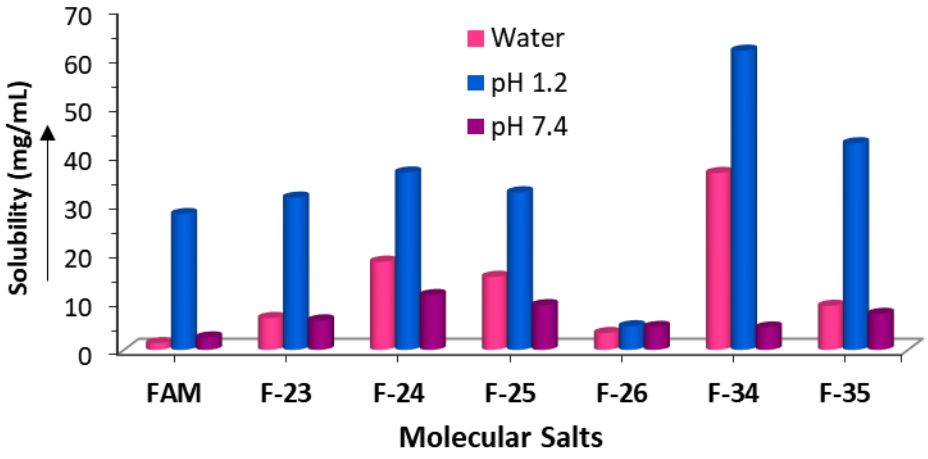

Figure 4.16 Comparison of solubility behavior of molecular salts F-23 to F-35 with its parent drug FAM in aqueous medium and buffer solutions of pH 1.2 and 7.4.

In an aqueous medium, the multicomponent solids displayed several-fold enhancement in the solubility in comparison to the FAM: F-23 (4.78-fold), F-24 (13.22-fold), F-25

(10.95-fold), F-26 (2.52-fold), F-34 (26.54-fold), and F-35 (6.60-fold). In a saline buffer solution of pH 1.2, the solubility of the salts is enhanced fairly except for F-26 whose solubility is 5.75-fold lower than that of the parent API. Interestingly, all the hydrated salts exhibited a higher solubility as compared to that of the anhydrous F-26. The reason for such higher solubility for hydrated complexes could be the inclusion of polar solvent molecules (H_2O) in their crystal lattice which causes a rise in the drug polarity, thereby increasing its interaction with the polar media (Figure 4.20). Apart from that the solubility of the crystalline material is usually inversely correlated with its melting point [27]. A similar relationship is observed for the FAM salts F-23 to F-35. The plot of the DSC melting endotherm shows lower melting points for the hydrated salts as compared to that of the anhydrous salt (Figure 4.2). Pure FAM has a melting point of 161–164 °C. All the hydrated salts melt at a lower temperature range of 110–130 °C, whereas the anhydrous F-26 salt melts at a higher temperature of 170–175 °C. The lowering of the melting point of the drug due to the formation of salt hydrates suggests the decrease of the lattice energy which can be also a reason for the better solubility.

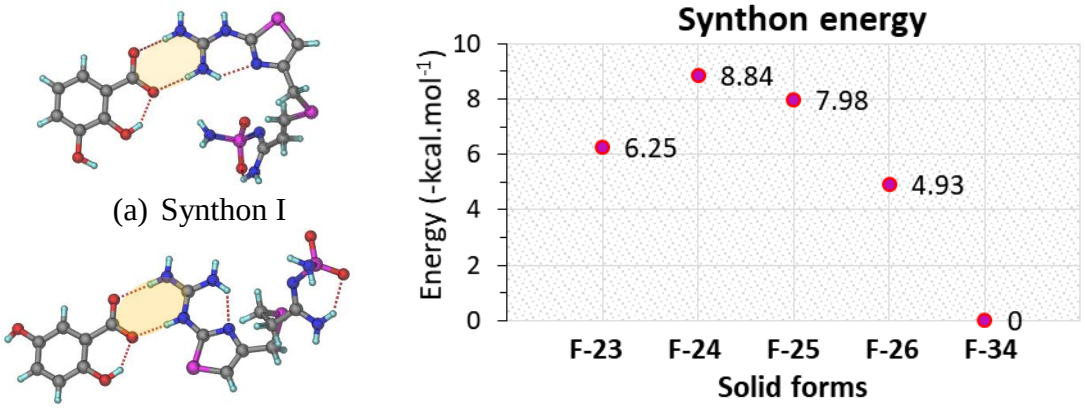

(a) Synthon I

(b) Synthon II

(c) Synthon energy

Figure 4.17 Prime hydrogen-bonded synthon observed in the structure of (a) F-23 and (b) F-24 to F-34. (c) The relative energy of synthon I and II. Unlike the other salts, COOH of the 35-DHBA in F-35 does not form a two-point synthon with the guanidine moiety of the FAM.

The solubility of multicomponent solids also depends on the strength of intermolecular interactions that are present between the drug and the coformer molecules. The synthon energy of prime hydrogen bonds in the crystal structure of these salts was computed to correlate with the solubility behavior. The calculation of the energy was performed on Gaussian09 using DFT with B3LYP; 6311G*(d, p) as the basic level, and the obtained relative values are plotted in Figure 4.17. As expected, the 34-DHBA coformer formed a

weaker hydrogen-bonded acid···guanidine two-point synthon with drug FAM (E = 0 kcal mol^{-1}) since it is the weakest acid among DHBAs with a p*K*a value of 4.26. The formation of such weaker drug–coformer interactions can be one of the reasons for the observed highest solubility for F-34. Though the acid···guanidine synthon formed in the crystal structure of F-23 and F-26 salts is weaker than that of the F-24 and F-25, the observed solubility of these salts is lower than that of the F-24 and F-25. In 1.2 pH and aqueous media, it is observed that the solubility of the molecular salts is generally inversely related to the coformer's acidity (see acidic strength of coformers in Table 4.3). The stronger the coformer acidity, the weaker will be its conjugated base. Hence, the coformer with stronger acidity affords salt of FAM with a weaker conjugated base. Such salt materials have a lower tendency to interact with the polar solvent and remain in their ionic state in low pH conditions, subsequently may exhibit lower solubility. For instance, the lowest solubility of F-26 observed at pH 1.2 is because 26-DHBA is the strongest acid among the coformers with the lowest p*K*a value of 1.51. Hence, the 2,6-hydroxybenzoate of F-26 is weaker and has a higher tendency to stay in its ionic state in acidic environments.

At pH 7.4, the multicomponent solids display enhanced solubility behavior as compared to the parent API but show a low and different solubility trend from that of the aqueous and pH 1.2 media. The increase in the solubility parameters is remarkable for pure API and its salts at pH 1.2 when compared with the values obtained from the aqueous and pH 7.4 media. The reason behind this is drug FAM can form hydrochloride salt in an acidic environment [28]. The interaction tendency of the ionized FAM with the polar solvent molecules increases, resulting in a higher solubility. Similarly, the solubility of molecular salts in the 1.2 pH condition is higher because of the presence of an acid proton in the buffer solution that can form a strong hydrogen bond with the anion of the molecular salts and enhances the solute-solvent interaction.

4.3.5 Membrane Permeation Behaviour

The membrane permeation property for the ground powder of product materials and the pure drug was determined at pH 1.2 and 7.4 conditions and plotted in Figures 2.18 and 2.19 respectively. In 1.2 pH, salt products demonstrate comparatively a better cumulative drug release and flux than the pure API, except for F-24 and F-26 which initially display a slower rate. A sharp increase in the amount of drug release and flux for products and

API is observed within 5 min except for F-26 (Figure 4.18. The permeation behavior of all products is higher than that of the pure API at pH 7.4 (Figure 4.19). But the permeation rate is slower at pH 7.4 as compared to that of the 1.2 pH condition.

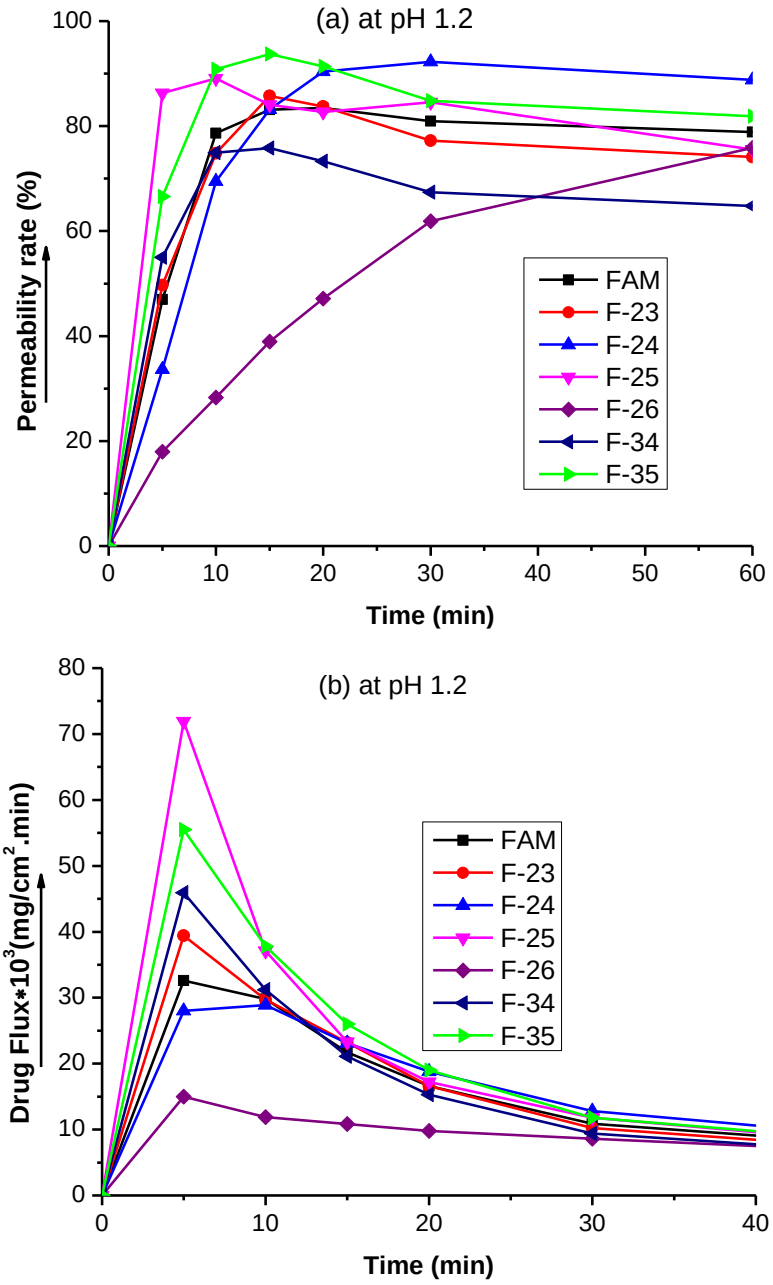

Figure 4.18 (a) Permeability rate and (b) drug flux of molecular salts and the parent drug at a buffer solution of pH 1.2.

The lowest permeation rate and drug flux observed at both pH 1.2 and 7.4 for anhydrous salt F-26 is because of its more ionic nature which could reduce the dissolution rate in the polar media, leading to a decrease in the concentration of the drug for permeation. On the other hand, salt hydrates display a higher permeation behavior in both pH 1.2 and 7.4 buffers. Because of the presence of water molecule(s) of crystallization, these hydrated

salts have lower lattice energy in comparison to the anhydrous F-26, resulting in higher solubility. As a result, the availability of a high concentration of drug in the absorption site creates high concentration gradients over the membrane and increases the permeation rate. FAM conformers extracted from the crystal structure of these salt hydrates with higher solubility and membrane permeability show conformation change in a narrow range in comparison to the other salts (Figure 4.13). A similar phenomenon was also observed for salts of FAM with mono-substituted benzoic acids [23].

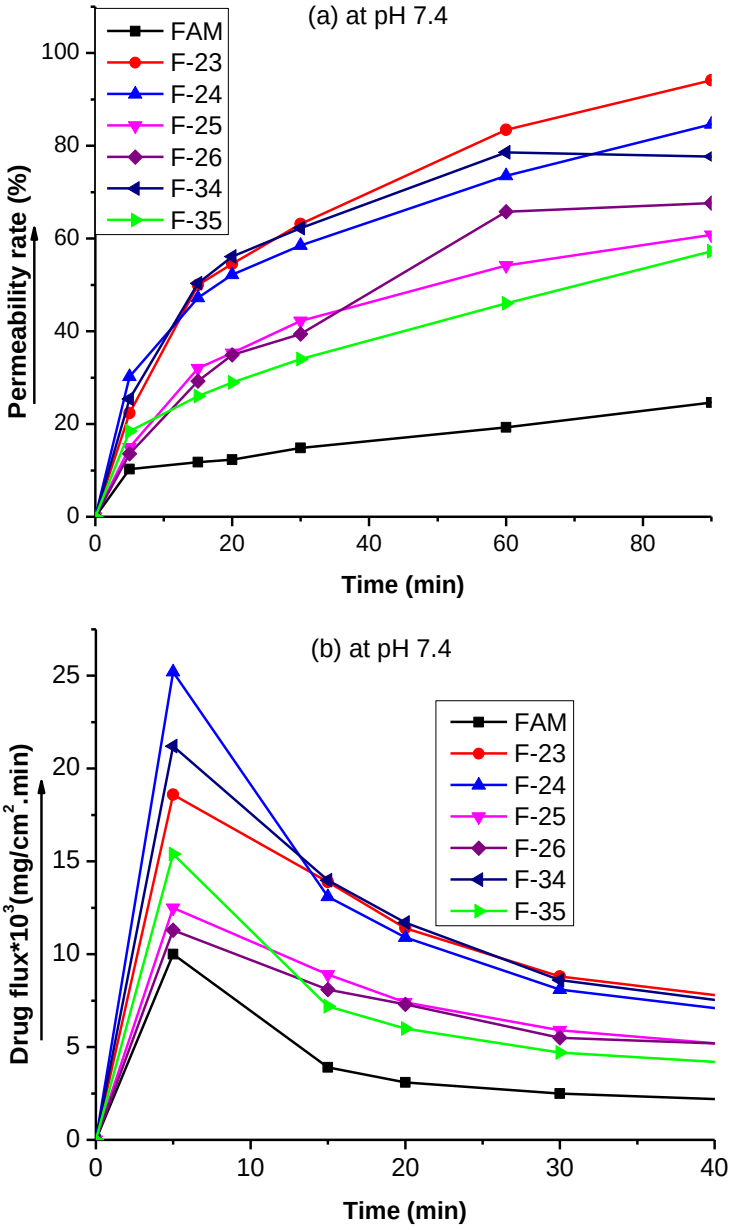

Figure 4.19 (a) Permeability rate and (b) drug flux of molecular salts and the parent drug at a buffer solution of pH 7.4.

4.3.6 Hirshfeld Surface Analysis

The noncovalent interactions that exist in the crystal lattice of solid materials play an important role in regulating the physicochemical properties of drug molecules. Increasing the polar nature of a drug by salt/cocrystal formulation usually enhances the solubility, but reduces the permeation rate because of its low lipophilicity in polar media. Hirshfeld surface analysis for product materials was carried out to comprehend how the isomeric positions of phenolic OH groups and water molecules of crystallization altered the lipophilicity of the drug, thereby the drug's properties. The diagram clearly shows that the percentage of polar O···H interaction for hydrated products (39.2–40.1%) is higher than that of the anhydrous product (29% for F-26). On the other hand, the percentage of less polar and nonpolar interactions, i.e., S···H and C···H, is lower for salt hydrates as compared to that of anhydrous salt (Figure 4.20). The inclusion of water molecule(s) in the crystal lattice of the salt products increased their polarity which in turn raised the solute···solvent interaction in the polar media and lead to higher solubility for the hydrated salts (Figure 4.16). At pH 7.4 condition, F-34 exhibits higher drug flux among dihydrate products. The percentage of polar O–H interaction for product F-34 (38.2%) is lower than that of the F-23 (39.6%) and F-35 (39.2%) which implies a lesser hydrophilic interaction for F-34 in the polar media leading to higher permeation. In addition to that a high percentage of hydrophobic C–H interaction (8%) renders a higher lipophilicity for F-34. The solubility and permeability parameters of F-25 were determined from the hydrated sample. F-25 is excluded from the comparison with the other salt hydrates since MeOH solvated crystal structure is used as input for the calculation of intermolecular interactions.

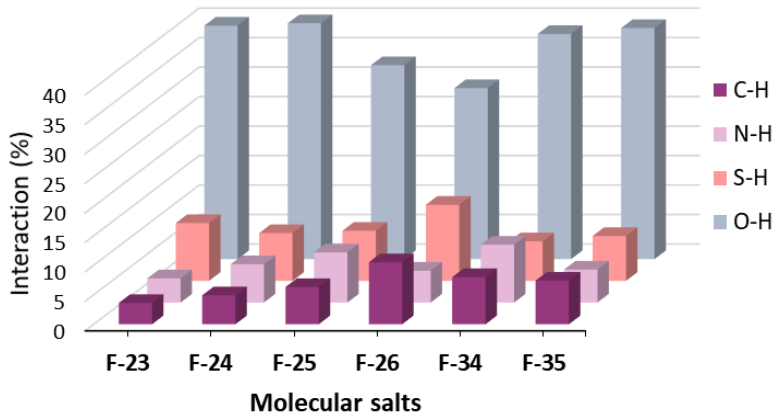

Figure 4.20 Comparison of various intermolecular interactions contribution in the product materials of FAM and DHBAs.

4.4 Summary

Multicomponent solid formulation of low bioavailable and unstable drug famotidine with the dihydroxybenzoic acids via mechanochemical grinding resulted in an anhydrous salt with 26-DHBA and hydrated salts with the remaining isomeric DHBA conformers. The anhydrous salt showed higher thermal stability than hydrated salts. Evaluation of the phase stability proved that all the products demonstrated higher drug stability in a highly acidic medium. The determination of the physicochemical properties in the different simulated stomach and intestinal fluids indicated that all hydrated salts exhibited superior solubility and membrane permeation behaviors than the parent API, whereas the formation of anhydrous salt with 26-DHBA reduced these physicochemical properties of the drug. The formation of guanidinium···carboxylate heterosynthon as a main intermolecular interaction has improved the drug properties. The variation in the isomeric position of phenolic OH groups of coformers and the inclusion of a water molecule of crystallization are responsible for the formation of different auxiliary hydrogen bonds and drug conformation change, which lead to the formation of a unique crystal packing with improved properties.

4.5 Experimental Section

4.5.1 Materials

Famotidine and the isomeric dihydroxybenzoic acids were purchased from Yarrow Chem Products, Mumbai, India, and alfa-aesar respectively. HPLC-grade solvents (MeOH and ACN) which were used for growing single crystals were obtained from SRL, India. Double-distilled and deionized water was used for the stability, solubility, and permeability experiments. All the chemicals and solvents were used as received from the suppliers.

4.5.2 Synthesis of Molecular Salts

All six molecular salts of FAM were prepared by the liquid-assisted grinding method. 1 mmol of FAM and 1 mmol of coformer were placed in the mortar and ground together with a few drops of water for about 30 min. Then the powder material was dissolved in solvents (MeOH or a mixture of MeOH and ACN) and kept at ambient conditions for crystallization. Single crystals were collected after 3–5 days and characterized using vibrational spectroscopy, thermal, and X-ray diffraction techniques.

4.5.3 Vibrational Spectroscopy

The IR spectra of the samples were recorded on the PerkinElmer Frontier MIR spectrophotometer (Figure 4.1). The major stretching vibrations frequencies (cm–1) for the API and its multicomponent products are presented as follows: FAM: 3508–3237 (N–H), 3103 (=C–H, alkene), 2936 (C–H, aliphatic), 1644−1603 (C=N), 1534 (C=C), 1288 & 1145 (SO2), 982 (N–S); F-23: 3425–3236 (N–H), 3108 (=C–H, alkene), 2919 (C–H, aliphatic), 1708 (C=N), 1631 & 1371 (COO^-), 1568 (C=C), 1266 &1140 (S=O), 950 (N–S); F-24: 3424–3228 (N–H), 3110 (=C–H, alkene), 2923 (C–H, aliphatic), 1702 (C=N), 1668 (N−H bending), 1630 & 1450 (COO^-), 1576 (C=C), 1310 & 1127 (S=O), 971 (N–S); F-25: 3582 (OH), 3408–3221 (N–H), 3118 (=C–H, alkene), 2931 (C–H, aliphatic), 1713 (C=N), 1625 & 1391 (COO^-), 1544 (C=C), 1338 & 1121 (S=O), 983 (N–S); F-26: 3412–3240 (N–H), 3109 (=C–H, alkene), 2923 (C–H, aliphatic), 1714 (C=N), 1630& 1389 (COO^-), 1584 (C=C), 1292 & 1118 (S=O), 986 (N–S); F-34: 3409–3251 (N–H), 3102 (=C–H, alkene), 2926 (C–H, aliphatic), 1698 (C=N), 1660 (N−H bending), 1626 & 1380 (COO^-), 1570 (C=C), 1283 & 1129 (S=O), 988 (N–S); F-35: 3508–3239 (N–H), 3104 (=C–H, alkene), 2928 (C–H, aliphatic), 1698 (C=N), 1607 & 1387 (COO^-), 1548 (C=C), 1288 & 1138 (S=O), 1004 (N–S).

4.5.4 Thermal Analysis

Differential scanning calorimetry (DSC) data were measured on Mettler Toledo DSC 822e model in a temperature range of 25−200 °C (Figure 4.2). Thermogravimetric analysis (TGA) of the samples was performed on the Mettler Toledo TGA/SDTA 851e module in the temperature range of 30–300 °C (Figure 4.3).

4.5.5 Powder X-ray Diffraction

PXRD data were recorded on a Bruker D8 Focus X-ray diffractometer, Germany using Cu-Kα X-radiation (λ = l.54056 Å) at 35 kV and 25 mA in the 2θ range 10–40° (Figure 4.4). Rietveld refinement using Powder Cell 2.3 software was done to compare the PXRD pattern of bulk material with the simulated PXRD profile extracted from the crystal structure (Figure A5, Appendix).

4.5.6 Single Crystal X-ray Diffraction

The Single Crystal X-RD data were collected on Bruker APEX-II CCD diffractometer using Mo Kα (λ = 0.71073 Å) radiation. The reduction of data was done by Bruker SAINT Software [29]. SADABS was employed for correcting the intensities of absorption. The crystal structure was solved and refined using SHELX-2014 [30]. Non-hydrogen atoms were refined anisotropically. The hydrogen atoms were placed on hetero atoms from electron density maps and C–H hydrogen atoms were located using the HFIX command in SHELX-TL. Packing diagrams and figures were plotted using the X-Seed software [31]. The hydrogen bond distance is neutron-normalized to its accurate neutron value of O–H 0.983 Å, N–H 1.009 Å, and C–H 1.083 Å and presented in Table 4.4. The summary of crystallographic data for these crystals is presented in Appendix Table A5 and the hydrogen bond parameters are listed in Table 4.4.

4.5.7 Cambridge Structural Database (CSD)

An overlay of FAM conformers extracted from the crystal structures of the molecular salts was drawn on Mercury4.1 linked to CSD 2022.1 software (Figure 4.12).

4.5.8 DFT Calculation

The energy values of the hydrogen-bonded synthons in the crystal structure of the molecular salt were calculated using Gaussian09 on DFT with B3LYP; 6311G *(d, p) as the basic level (Figure 4.17c).

4.5.9 Hirshfeld Surface Analysis

The contribution percentage of various intermolecular interactions salts were calculated using Crystal Explorer version 21 at the B3LYP/6-31G *(d, p) level of theory (Figure 4.20).

4.5.10 Phase Stability Study

The phase stability of the product materials was evaluated by performing the slurry experiments. The details are in the experimental section 3.5.11 of Chapter 3.

4.5.11 Solubility Study

The solubility experiments were done in three different pH conditions (Figure 4.16). An excess amount of powder material was added to 3 mL of pure water or buffer solutions and stirred at 1000 rpm for 12 h. The pH change during the solubility study was checked

and remained unchanged up to 12 h. The filtered aliquots were diluted and their absorbance was measured on an Agilent Cary-60 double beam UV–vis spectrophotometer at the ambient temperature of 25 °C. The unknown concentration of filtered aliquots of product materials (Cu) was calculated from the calibration curves of standard solutions using the formula Cu = (Au – intercept)/slope, where Au is the absorbance of the unknown solution.

4.5.12 Membrane Permeability Study

The membrane permeability experiment was carried out through dialysis membrane-135 in a diffusion apparatus following the procedures reported in the literature [32,33]. 5 mg of ground powder material was placed in the membrane and enclosed with clips as a donor compartment and suspended in the receptor compartment containing 100 mL of solutions (pH = 1.2/7.4.) The solution was stirred at 800 rpm at ambient conditions (26 °C) and the sample was allowed to diffuse through the membrane toward the receptor compartment. Three milliliters of the sample were extracted from the receptor compartment at a definite time interval. The volume of solution in the receptor compartment was kept constant by the addition of the same volume of fresh solution each time. The amount of sample diffused through the membrane was determined by measuring the absorbance of the solution using UV–vis spectrophotometry for each time interval.

4.6 References

[1] Langtry, H. D., Grant, S. M., and Goa, K. L. Famotidine. *Drugs*, 38(4):551-590, 1989.

[2] Berry, D. J. and Steed, J. W. Pharmaceutical cocrystals, salts, and multicomponent systems; intermolecular interactions and property based design. *Advanced drug delivery reviews*, 117:3-24, 2017.

[3] Chen, J., Sarma, B., Evans, J. M. B., and Myerson, A. S. Pharmaceutical crystallization. *Crystal growth & design*, 11(4):887-895, 2011.

[4] Nangia, A. K. and Desiraju, G. R. Heterosynthons, Solid Form Design and Enhanced Drug Bioavailability. *Angewandte Chemie*, 134(39):e202207484, 2022.

[5] Smith, A. J., Kavuru, P., Wojtas, L., Zaworotko, M. J., and Shytle, R. D.

Cocrystals of quercetin with improved solubility and oral bioavailability. *Molecular pharmaceutics*, 8(5):1867-1876, 2011.

[6] Moody, C. L. and Wheelhouse, R. T. The medicinal chemistry of imidazotetrazine prodrugs. *Pharmaceuticals*, 7(7):797-838, 2014.

[7] Taylor, L. S., Braun, D. E., and Steed, J. W. Crystals and Crystallization in Drug Delivery Design. *Molecular Pharmaceutics*, 18(3):751-753, 2021.

[8] Thakuria, R. and Sarma, B. Drug-drug and drug-nutraceutical cocrystal/salt as alternative medicine for combination therapy: a crystal engineering approach. *Crystals*, 8(2):101, 2018.

[9] Saikia, B., Pathak, D., and Sarma, B. Variable stoichiometry cocrystals: occurrence and significance. *CrystEngComm*, 23(26):4583-4606, 2021.

[10] Karki, S., Friščić, T., Fabian, L., Laity, P. R., Day, G. M., and Jones, W. Improving mechanical properties of crystalline solids by cocrystal formation: new compressible forms of paracetamol. *Advanced materials*, 21(38-39):3905-3909, 2009.

[11] Bora, P., Pathak, D., Kalita, B. K., and Sarma, B. Deciphering the Role of Environmental Variables in the Nucleation of Stoichiometric Cocrystals. *Crystal Growth & Design*, 23(3):1500-1510, 2023.

[12] Bolla, G., Sarma, B., and Nangia, A. K. Crystal Engineering of Pharmaceutical Cocrystals in the Discovery and Development of Improved Drugs. *Chemical Reviews*, 122(13):11514–11603, 2022.

[13] Évora, A. O. L., Castro, R. A. E., Maria, T. M. R., Rosado, M. T. S., Ramos Silva, M., Matos Beja, A., Canotilho, J., and Eusébio, M. E. S. Pyrazinamide-diflunisal: a new dual-drug co-crystal. *Crystal growth & design*, 11(11):4780-4788, 2011.

[14] Gopi, S. P., Ganguly, S., and Desiraju, G. R. A drug–drug salt hydrate of norfloxacin and sulfathiazole: Enhancement of in vitro biological properties via improved physicochemical properties. *Molecular pharmaceutics*, 13(10):3590-3594, 2016.

[15] Nugrahani, I., Asyarie, S., Soewa, S. N., and Ibrahim, S. The antibiotic potency of amoxicillin-clavulanate co-crystal. *International Journal of Pharmacology*,

3(6):475-481, 2007.

[16] Cherukuvada, S., Babu, N. J., and Nangia, A. Nitrofurantoin–p-aminobenzoic acid cocrystal: Hydration stability and dissolution rate studies. *Journal of pharmaceutical sciences*, 100(8):3233-3244, 2011.

[17] Suresh, K., Goud, N. R., and Nangia, A. Andrographolide: solving chemical instability and poor solubility by means of cocrystals. *Chemistry–An Asian Journal*, 8(12):3032-3041, 2013.

[18] Sarma, B. and Saikia, B. Hydrogen bond synthon competition in the stabilization of theophylline cocrystals. *CrystEngComm*, 16(22):4753-4765, 2014.

[19] Mittapalli, S., Bolla, G., Perumalla, S., and Nangia, A. Can we exchange water in a hydrate structure: a case study of etoricoxib. *CrystEngComm*, 18(16):2825-2829, 2016.

[20] Zhu, B., Wang, J.-R., Zhang, Q., and Mei, X. Improving dissolution and photostability of vitamin K3 via cocrystallization with naphthoic acids and sulfamerazine. *Crystal Growth & Design*, 16(1):483-492, 2016.

[21] Yang, D., Cao, J., Jiao, L., Yang, S., Zhang, L., Lu, Y., and Du, G. Solubility and stability advantages of a new cocrystal of berberine chloride with fumaric acid. *ACS omega*, 5(14):8283-8292, 2020.

[22] Saikia, B., Sultana, N., Kaushik, T., and Sarma, B. Engineering a Remedy to Improve Phase Stability of Famotidine under Physiological pH Environments. *Crystal Growth and Design*, 19(11):6472-6481, 2019.

[23] Zeleke, T. Y. and Sarma, B. Isomeric Coformer Responsive Conformational Adjustment to Recuperate Stability, Solubility, and In Vitro Permeation Behavior of Drug Molecular Salts. *Crystal Growth & Design*, 22(12):7405–7418, 2022.

[24] Reutzel-Edens, S. M., Braun, D. E., and Newman, A. W. *Hygroscopicity and Hydrates in Pharmaceutical Solids*. Vol 2. Wiley-VCH; 2018.

[25] Bora, P., Saikia, B., and Sarma, B. Regulation of π···π Stacking Interactions in Small Molecule Cocrystals and/or Salts for Physiochemical Property Modulation. *Crystal Growth & Design*, 18(3):1448-1458, 2018.

[26] Maity, D. K., Paul, R. K., and Desiraju, G. R. Drug–drug binary solids of nitrofurantoin and trimethoprim: crystal engineering and pharmaceutical properties. *Molecular Pharmaceutics*, 17(12):4435-4442, 2020.

[27] Khatioda, R., Bora, P., and Sarma, B. Trimorphic ethenzamide cocrystal: in vitro solubility and membrane efflux studies. *Crystal Growth & Design*, 18(8):4637-4645, 2018.

[28] Ishida, T., In, Y., Inoue, M., and Yanagisawa, I. Structural study of histamine H2-receptor antagonists. Five 3-[2-(diaminomethyleneamino)-4-thiazolylmethylthio] propionamidine and-amide derivatives. *Acta Crystallographica Section B: Structural Science*, 45(5):505-512, 1989.

[29] *SAINT Plus (v 6.14); Bruker AXS Inc. Inc., Madison, WI*. 20082008.

[30] *SAINT Plus, Bruker AXS Inc.: Madison, WI*. 2008.

[31] Barbour, L. J. X-Seed, graphical interface to SHELX-97 and POV-Ray. *University of Missouri-Columbia, Columbia, MO*, 1999.

[32] Saikia, B., Bora, P., Khatioda, R., and Sarma, B. Hydrogen Bond Synthons in the Interplay of Solubility and Membrane Permeability/Diffusion in Variable Stoichiometry Drug Cocrystals. *Crystal Growth and Design*, 15(11):5593-5603, 2015.

[33] Sanphui, P., Devi, V. K., Clara, D., Malviya, N., Ganguly, S., and Desiraju, G. R. Cocrystals of Hydrochlorothiazide: Solubility and Diffusion/Permeability Enhancements through Drug–Coformer Interactions. *Molecular Pharmaceutics*, 12(5):1615-1622, 2015.